SCANNING VOL. 30, 232–239 (2008)

Evaluation of Surface Roughness and Nanostructure of Indium Tin Oxide (ITO) Films by Atomic Force Microscopy

G. KAVEI, Y. ZARE and A. MOHAMMADI GHEIDARI

Material and Energy Research Center (MERC), Tehran, Iran

Summary: Indium tin oxide was deposited on a glass (soda lime glass) by radiofrequency sputtering system at different sputtering gas (argon/oxygen 90/10%) pressures (20–34 mTorr) at room temperature. The sputtering rate was affected by the sputtering gas pressure. The optimum sputtering gas pressure was found to be 27 mTorr. The samples at different thicknesses (168, 300, 400, 425, 475, 500 and 630 nm) were deposited on the substrate. Transparency, electrical conductivity and surface roughness of the films were characterized. The samples were annealed at 350, 400 and 450°C to evaluate annealing process effects on the concerned parameters and, therefore, the above-mentioned measurements were repeated again. The films exhibited reasonable optical transmittance and electrical conductivity and greatly improved after annealing. The characterization was focused on the scanning of the film surfaces before and after annealing, which has a prominent effect on the optical properties of the films. Film surfaces were scanned by scanning probe microscopy in contact atomic force mode. The most consideration was devoted to image analysis. SCANNING 30: 232–239, 2008. © 2008 Wiley Periodicals, Inc.

Key words: scanning probe microscopy (SPM), atomic force microscopy (AFM), transparent conducting oxide (TCO), image analysis

Address for reprints: G. Kavei, Material and Energy Research Center (MERC), P.O. Box 14155-4777, Tehran, Iran, E-mail: g-kavei@merc.ac.ir or ghassem113@yahoo.com

Received 12 November 2007; Accepted with revision 12 March 2008

DOI 10.1002/sca.20104
Published online 30 May 2008 in Wiley InterScience (www.interscience.wiley.com)

Introduction

Transparent conducting oxides were of interest to scientists since 1907, when reports of transparent and conductive cadmium oxide (CdO) films were first published by Badeker (1907). Since then there has been a growing technological interest in materials with these unique properties as evidenced by not only their increased number but also the large variety of techniques developed for depositing them. It is now fairly known that nonstoichiometric and doped films of oxides of tin, indium, cadmium, zinc and their various alloys exhibit high transmittance and nearly metallic conductivity (Chopra *et al.* 1983, Tiwari *et al.* 1987).

Although partial transparency, with normal reduction in conductivity, can be obtained for many thin metallic films, high transparency and high conductivity cannot be attained simultaneously in intrinsic stoichiometric materials. The only way is to create electron degeneracy in a wide band-gap material ($E_g > 3$ eV or more for visible radiation) by controllably introducing nonstoichiometry and/or appropriate dopants. These conditions can be conveniently met for indium tin oxide (ITO) as well as for a few other materials mentioned above (Nath and Bunshah 1980).

Nowadays, the technology of optical sensors and solar cells is being considered more and more important (Terzini *et al.* 2000, Guillen and Herrero 2006, Kerkach *et al.* 2006). ITO, deposited on a transparent glass, has many advantages for sensors and solar cells, including good mechanical and optical properties. It is also a good electrical insulator and can be bound easily to silicon substrates at room temperature (lower than the temperature needed for fusion bonding).

However, ITO with reported transmittance and conductivity as high as 5% and $10^4/\Omega\,\mathrm{cm}$, respectively, is the most popular material for electronic and optoelectronic applications (Minami 2008). It is essentially formed by the substitutional doping of In_2O_3 with Sn, which replaces In^{3+} atoms from the

cubic bixbyite structure of indium oxide (Fan and Goodenough 1977). ITO films have lattice parameter close to that of In_2O_3, which lies within the range of 10.2–10.31 Å (Nath and Bunshah 1980). Thus, Sn forms an interstitial bond with oxygen either at SnO or SnO_2 forms, with a valence of +2 or +4, respectively. This valence state plays an important role in the conductivity of ITO. The lower valence state results in reduction in carrier conductivity. When a hole is created, it acts as a trap and reduces the conductivity. The existence of the SnO_2 state means the existence of Sn^{4+}, which implies that SnO_2 acts as an n-type donor. Nevertheless, in ITO, both substituted tin and oxygen vacancies result in high conductivity, and the formula of the compound is represented as $In_{2-x}Sn_xO_{3-2x}$.

There are different ways to enhance the efficiency of some optical devices such as solar cells, sensors, etc. In one of these methods, light is allowed to have more reaction with the material by roughening the surface. Reliable roughness is obtained by annealing the sample. As wave scattering depends on the morphology of rough surfaces, it is an important parameter on ITO films, especially when used as solar cells. Hence, surface characterization plays an important role on the effective properties of optoelectronic devices fabricated by ITO films. A summary of electrical and optical properties of typical ITO films deposited using various techniques is reported by Bashar (1997).

In recent years, scanning probe microscopy (SPM) has become a valuable system to measure and discern the surface properties such as roughness, electrical and magnetic parameters of materials in small scales. In particular, microscopes equipped with powerful softwares, such as image analyzing softwares, promote the extraction of necessary data needed to interpret the experiment results in detail. In this system, atomic force microscopy (AFM) method characterizes the profile of surface morphology and its nanostructure at high precision (Bruce 1997, Barabasi and Stanley 1995, Jafari *et al.* 2003). Generally, in the AFM method, the contact atomic force microscopy (C-AFM) mode is selected to study the semiconductor surfaces; in this mode the tip–sample contact area is minimum, providing the highest resolution (subnanometer) in imaging of stochastic topographical features. The height on the images (Z), recorded in C-AFM, also represents the most accurate, true topography of soft samples.

Experimental

Layers with various thicknesses (168, 300, 400, 425, 475, 500 and 630 nm) were deposited on cleaned substrates (soda lime glass) by radio-frequency (RF) sputtering system at room temperature. A commercial sample of ITO, which is a ceramic with (In_2O_3/SnO_2: 90/10%), was placed as the target of sputtering. The system was evacuated up to $\sim 10^{-5}$ Torr before sputtering. For all deposition steps, the target (In_2O_3/SnO_2: 90/10%) was presputtered for 15 min in the selected sputtering condition to warranty the purity of ITO deposited on the substrate. To prepare a plasma medium for sputtering (argon/oxygen: 90/10%), gas was admitted into the system, increasing the vacuum pressure to $\sim 10^{-3}$ Torr. The mixed gas collided with the target at a rate of 10^{-3} cm^3/min at a voltage of 10 kV and the measured sputtering power of 350 W, depositing the ITO on the substrate (soda lime glass that can tolerate a temperature as high as 500 °C). Surface resistance and light transmission properties were measured by the method of Mohammadi Gheidari *et al.* (2007) and the structure of the surface roughness was evaluated by SPM.

Force interaction between the C-AFM tip and the sample surface must be minimized for non-destructive imaging and convoluted features of the samples. This is performed (a) by means of a particular mode of AFM imaging, which allows exploration of surface without damage or alteration and (b) by selecting an appropriate tip depending on the degree of the surface roughness, provided the tips for AFM imaging prevent surface damage by eliminating the lateral forces that are inherent in contact mode (where the tip is simply dragged over the surfaces).

The AFM used in this study was Solver Pro (NT-MDT Ltd., Moscow, Russia) operating in the C-AFM mode. The tips used were silicon nitride CG01S, manufactured by MDT, compatible with most of the SPM devices with a nominal force constant of 0.03 N/m. To capture the images, the samples were mounted carefully on the sample holder by a two-sided adhesive Selo tape. This type of mounting causes a tilt that screens severely the structures of the surface. To eliminate such a deficiency and to expose the structures, images were manipulated using flattening second-order processing software proposed with the SPM system. The acquired structure of the surface is very sensitive to the degree of this correction; the more the manipulation, the less accurate the result. Therefore, an optimum order has to be selected. In this study, after careful mounting of the samples, second-order flattening of the images was found to be optimum.

Samples were annealed under a pressure of 10^{-5} Torr. Annealing is a gently warming up process at a suitable environment (low-pressure inert gas media). Samples were warmed up to 200, 300, 350, 380, 400 and 450 °C at a vacuum of 10^{-5}–10^{-4} Torr.

In order to realize the postannealing effect on the physical, structural and electro-optical properties of the films, structural properties were studied by means of X-ray diffraction (XRD) and SPM techniques once more. The optical transmission and sheet resistance of the films were measured by a spectrophotometer and a four-point probe technique. Some physical properties of the films were also taken from the XRD and transmission data.

Results and Discussions

Deposited Samples

Figure 1 shows the XRD analysis of some selected samples prepared at sputtering gas pressures of 24, 27, 30 and 34 mTorr at 400 °C. In this figure, the main growth directions are (222), (400), (440) and (622), which are related to the cubic structure of In_2O_3 as reported by Hu *et al.* (2004). It was also quoted by Terzini *et al.* (2000) that for the films deposited at sputtering pressures of 20–24 mTorr at 400 °C, the ratio of the intensity of (222) peak to that of (400) (i.e., I_{222}/I_{400}) is 5 times (or even more) the standard value of the ratio for ITO powder. Therefore, the most part of the layer parallel to the surface has been textured in the ⟨111⟩ direction, whereas for films deposited at a sputtering pressure of 25–34 mTorr this ratio is much less than the standard value, resulting in the ⟨100⟩ direction textured films (Terzini *et al.* 2000). The lattice parameter (calculated from XRD strongest peak) and interplaner distances (*d*) of the film are summarized by Mohammadi Gheidari *et al.* (2007). It was concluded that as the film growth is in progress, the films are under tensile stress. For the films prepared at high sputtering power and room temperature, the larger value of the lattice parameter can

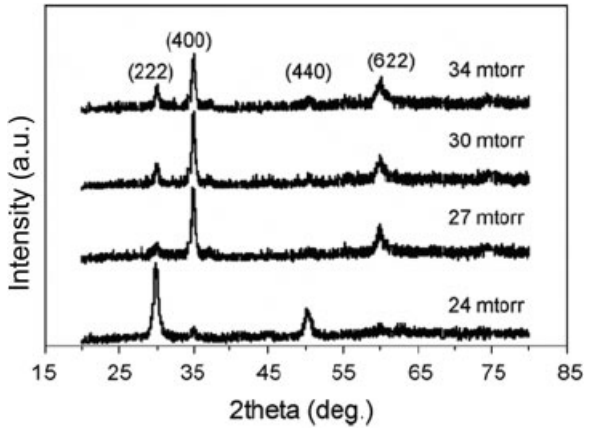

Fig 1. XRD analysis of ITO films prepared at sputtering gas pressures of 24, 27, 30 and 34 mTorr at 400 °C. XRD = X-ray diffraction, ITO = indium tin oxide.

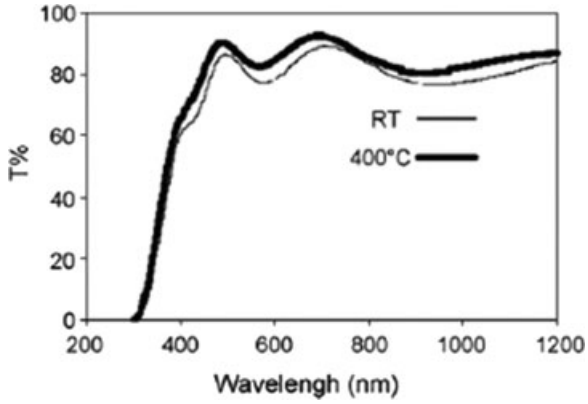

Fig 2. Transmittance spectra from the films just deposited (room temperature) and 400 °C annealed. Films were deposited in the system at 27 mTorr pressure.

fairly be attributed to the introduction of Sn atoms into the crystal lattice (Kerkach *et al.* 2006). The lattice parameters and the plane distances decrease with increase in sputtering pressure from 20 to 34 mTorr. This is attributed to the higher oxygen vacancies at higher sputtering pressure and antisite defects in the structure (Horák *et al.* 2007).

Transmission spectra of the films deposited at 27 mTorr sputtering gas pressure at two different temperatures are shown in Figure 2. The raise in energy gap for the films deposited at sputtering gas pressure of 27 mTorr is attributed to the structure, roughness variation and increasing oxygen vacancy (Terzini *et al.* 2000, Kerkach *et al.* 2006). However, the films deposited at different sputtering gas pressures have different thicknesses (Mohammadi Gheidari *et al.* 2007). The thicker film has a rough surface as shown in Figure 3 and as discussed by Jafari *et al.* (2007) it has low transmission and electrical conductivity; this fact is well supported by the film's resistivity variation study (Barabasi and Stanley 1995). Taking these assumptions into consideration, the average transmissions (T_{ave}) in the visible region of the spectrum and the film's resistivity may be determined (Mohammadi Gheidari *et al.* 2007). The conclusions of the calculations for deposited samples are as follows: at asputtering gas pressure from 20 to 27 mTorr, the average transmission increases with sputtering pressure, but any increment in sputtering pressure from 27 to 30 mTorr decreases the average transmission by 82% (for 27 mTorr). Increasing the sputtering gas pressure from 20 to 30 mTorr decreases the film resistivity.

Annealed Samples

Figure 4 shows the XRD spectra of some selected samples prepared with a thickness of 300 nm

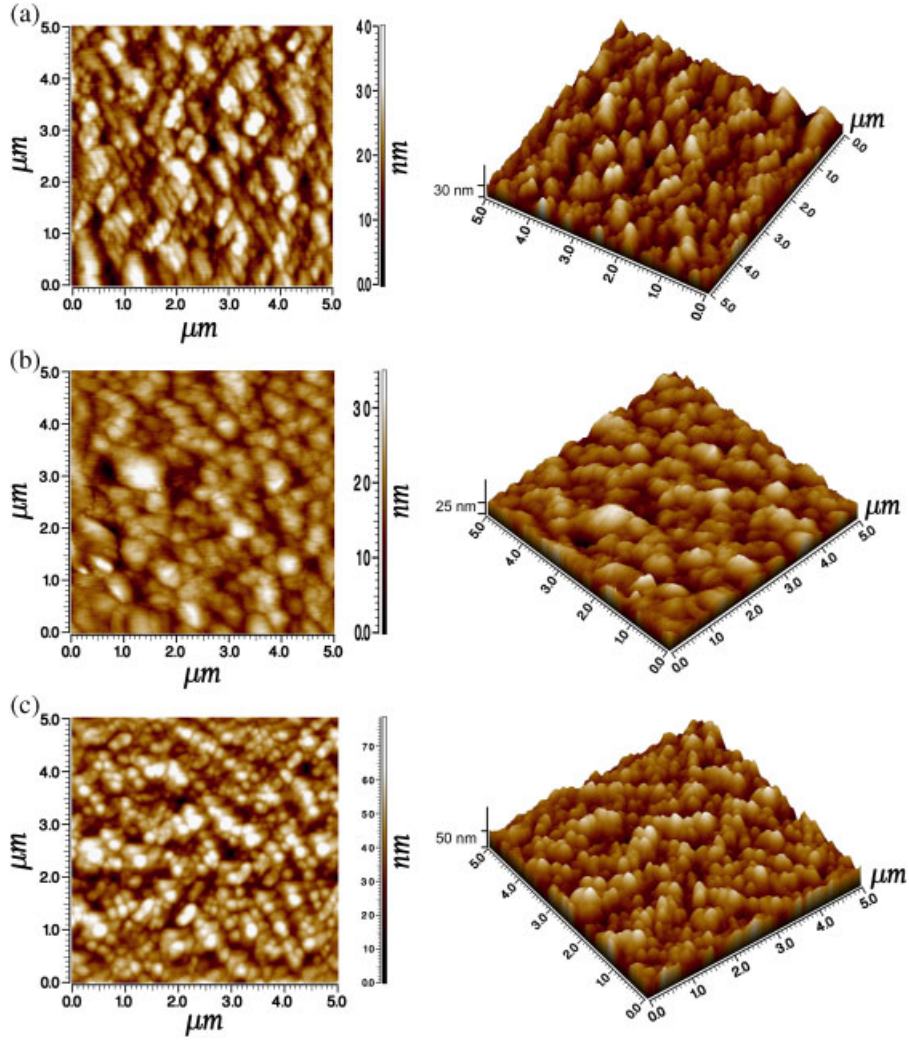

Fig 3. The surface roughness against film thicknesses: (a) 425 nm; (b) 475 nm; (c) 630 nm at room temperature. The thicker film has a rough surface.

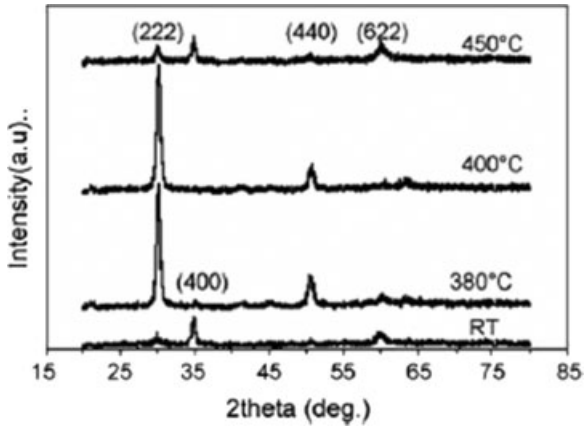

Fig 4. XRD analysis of the films with a thickness of 300 nm and a sputtering gas pressure of 27 mTorr at room temperature and annealed at 380, 400 and 450 °C. XRD = X-ray diffraction.

and a sputtering gas pressure of 27 mTorr at room temperature, 380, 400 and 450 °C, respectively. In this figure, the variation of the (222) and (400) peak intensities for the films vs. annealing temperature is demonstrated. The (400) peak disappears with an increase in the annealing temperature up to 400 °C and reappears at 450 °C, whereas the intensity of the (222) peak behaves inversely. The variation of the (222) and (400) crystallite sizes (from XRD data), lattice parameter and interplaner distance (d) for the (222) and (400) crystal planes are presented in Table I. The (400) oriented crystallites are larger in intensity than (222). Such films have a scattered nature depending on the annealing temperature. The size of the (222) crystallites increases with an increase in the annealing temperature and takes a maximum value of 26.2 nm at 400 °C. The interplaner distance, d, for the (222) crystal planes decreases systematically with an increase of temperature to 400 °C. This means that the film favors to release its stress along the [111] direction during annealing and at 400 °C it has a minimum value of stress.

TABLE I. The relative intensity of the (222)/(400), interplaner distances, average optical surface resistivity and transmission of the films in various annealing temperatures

No.	Annealing temp. (°C)	(222) Intensity relative to (400)	Interplaner distances (d) (Å)	Surface resis. ($\Omega\,cm^2$)	Average transmission (%)
1	Room	Amorphous	Amorphous	1k	24
2	200	0.14	2.982	301	83
3	300	0.51	2.980	89	80
4	400	1	2.954	17	86
5	450	0.66	2.961	45	86

TABLE II. Statistical parameters, calculated in the roughness analysis mode

Amount of sampling	The number of points, equal to $xyN_x{*}N_y$
Z_{max}	Maximal height
Z_{min}	Minimal height
Peak-to-peak, R_y	Peak-to-peak value, ISO 4287/1 (nm)
Ten-point height, R_z	$R_z = 1/5(Z_{max1}+Z_{max2}+Z_{max3}+Z_{max4}+Z_{max5}-Z_{min1}-Z_{min2}-Z_{min3}-Z_{min4}-Z_{min5})$, ten-point height, ISO 4287/1. The parameter expresses the surface roughness by the selected five maximal heights and hollows (nm)
Average roughness, R_a	Average roughness, ISO 4287/1 (nm)
Root mean square (RMS), R_q	Root mean square roughness, ISO 4287/1 (nm)
Surface skewness, R_{sk}	The asymmetry (the third central moment μ_3) characterizes the nonsymmetry of distribution. If the asymmetry is different from zero, the distribution is nonsymetrical The asymmetry equals zero for the symmetrical (relative to the center) distribution. The asymmetry is positive if the distribution is excessive on the right and negative if the distribution is excessive on the left
Coefficient of kurtosis, R_{ka}	The excess (surface kurtosis, the fourth central moment μ_4) characterizes the distribution spread

$Z_{ij} = Z(X_iY_j)$ is a discrete function, set on XY plane, whereas N_x, N_y is the number of points on the X, Y-axes.

Definition of the Roughness Parameters

The roughness parameters are determined on each image obtained in the tapping mode (height image) and are defined as follows:

R_q is the standard deviation of the Z values within a given area and is calculated using

$$R_q = \left[\sum (Z_i - Z_{ave})^2/N\right]^{1/2}$$

where Z_{ave} is the average of the Z values within the given area, Z_i the current Z value and N the number of points within the given area.

R_a is the mean roughness. This is the mean value of the surface fluctuations relative to the center plane and is calculated using

$$R_a = 1/L_xL_y \int_0^{L_y}\int_0^{L_x} |f(x,y)|\,dx\,dy$$

where $f(x,y)$ is the surface fluctuation relative to the center plane and L_x and L_y are the dimensions of the surface.

In order to express the surface roughness effect on the samples properties, the explanation related to the surface fluctuations of the flattened images captured from just deposited and annealed films was compared using SPM. Figure 5(a) is the AFM 2-D image of the sample with a thickness of 630 nm and with no thermal process on the sample. The image is just captured during a real-time operation (raw image) as off-line commands. Figure 5(b) shows the 3-D image and (c) is a profile of the fluctuation on the surface along the line shown in (a). Figure 6(b) is the flattened, processed image depicted in Figure 5. Figure 6(a) shows the surface constituents as fine grains of probably ITO and the much closed boundary grains. In Figure 6(b) and (c), the 3-D image and profiles of surface roughness are also shown to give a high prospectus from the surface. Figure 7(a) illustrates the 2-D image of the same sample after thermal operation in which the sample was heated up to 400 °C. Thermal modification enlarges the boundary grains (which can be clearly seen in the image) and results in improved electrical conductivity and optical properties. Again, Figure 7(b) and (c) has been included to show a clear view of the fluctuations of the surface. The films have a granular structure and the grain sizes in this image are larger than those calculated from XRD spectra (26.2 nm). By AFM analysis, the size of some grains was evaluated: they had sizes in the range of 35–40 nm. Statistical parameters,

TABLE III. Comparison of data from the raw and flattened images shown in Figures 5 and 6

	Data obtained from raw image	Data obtained from flattened image
Amount of sampling	65,536	65,536
Max = Z_{max}	34.6614 (nm)	29.589
Min = Z_{min}	0 (nm)	0
Peak-to-peak, R_y	34.6614 (nm)	29.589
Ten-point height, R_z	17.4998 (nm)	14.9044
Average	17.7534 (nm)	15.5553
Average roughness, R_a	3.46366 (nm)	3.08446
Second moment	18.2792	16.0326
Root mean square, R_q	4.3529 (nm)	3.88311
Surface skewness, R_{sk}	−0.165999	−0.18632
Coefficient of kurtosis, R_{ka}	0.0309446	0.0419823
Entropy	7.72476	7.55948
Redundance	−0.522713	−0.562719

calculated in the roughness analysis mode, are listed in Table II to give a clear view of the obtained data listed in Table III from Figures 5 and 6 for surface roughness analysis.

The effects of the annealing processes on the optical transmission of the deposited films are shown in Figure 2. In this figure, the optical transmission spectra of visible and near-IR spectrum for just deposited films annealed at 400 °C are shown. The relative intensity of the (222)/(400), interplaner distances, average optical surface resistivity and transmission of the films in various annealing temperatures are also summarized in Table I. The surface resistivity of the films takes its minimum value at 400 °C along with transmission enhancement, which is attributed to larger carrier mobility, film crystallite improvement and grain size enlargement at this temperature (Barabasi and Stanley 1995, Jafari *et al.* 2003, Bashar 1997, Mohammadi Gheidari *et al.* 2007, Hu *et al.* 2004, Vassant Kumar and Mansingh 1989, Aggour *et al.* 2000).

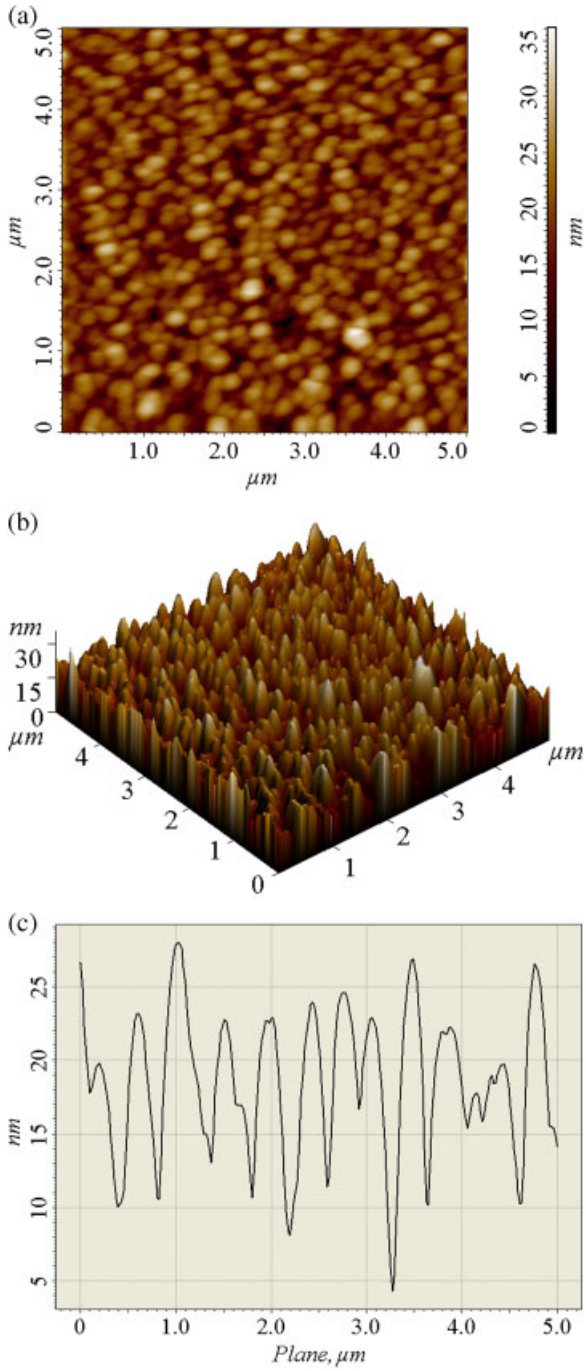

Fig 5. (a) The 2-D image from the sample with a thickness of 630 nm just deposited (raw image). (b) and (c) 3-D image and the profile of the fluctuations of the surface roughness along the line shown in (a), respectively.

Conclusions

ITO thin films have been deposited onto soda lime glass substrates by RF sputtering at different sputtering gas pressures (20–34 mTorr). The deposition rate increased by an increase in the sputtering gas pressure up to 30 mTorr and decreased above 30 mTorr. The film's crystal orientation changed from [111] to [100] as the sputtering gas pressure exceeded 24 mTorr. The sputtering gas pressure of 27 mTorr, leading to good combined electrical conductivity and optical transparency, was used to deposit the films and these films were annealed at different temperatures in vacuum. The surface roughness study reveals that the grains were well arranged at 400 °C and therefore had lowest scattering coefficient. However, the annealing temperature of 400 °C leads to better conductivity and transparency, larger grain size and lower stress for the films. In order to express the optoelectronic properties on the surface roughness, the explanation related to the surface fluctuations of the flattened

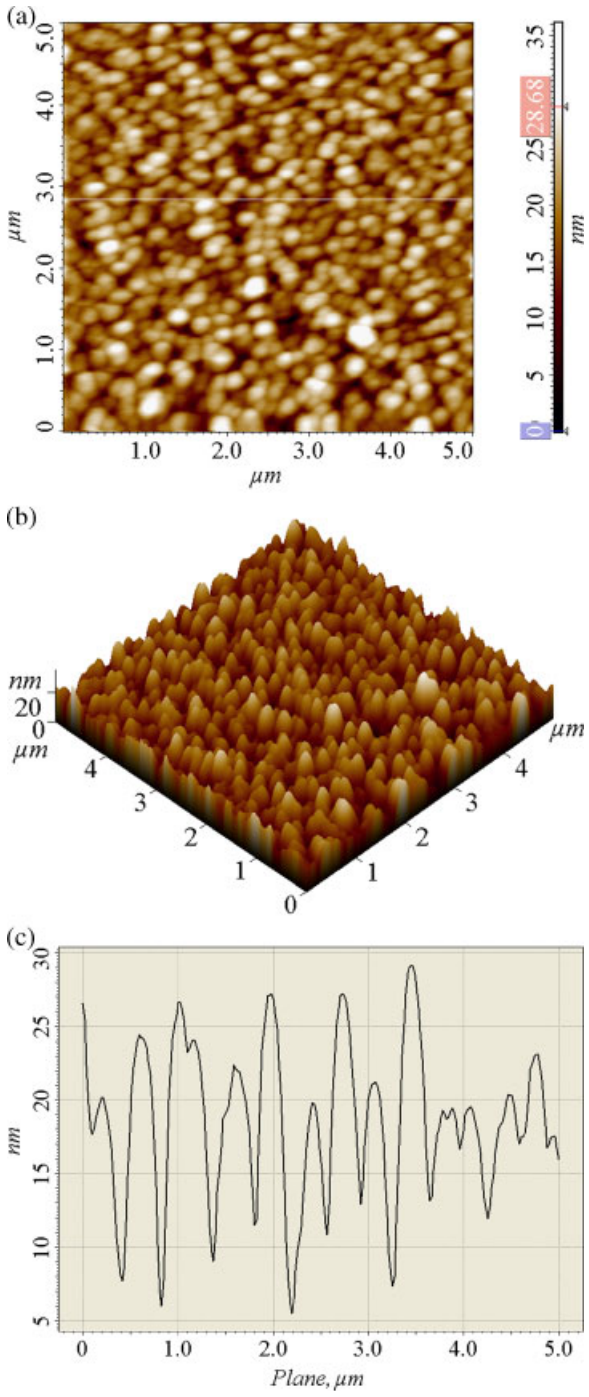

Fig 6. (a) The 2-D image from the sample with a thickness of 630 nm after the flatting process. (b) and (c) The 3-D image and the profile of the fluctuations of the surface roughness, respectively.

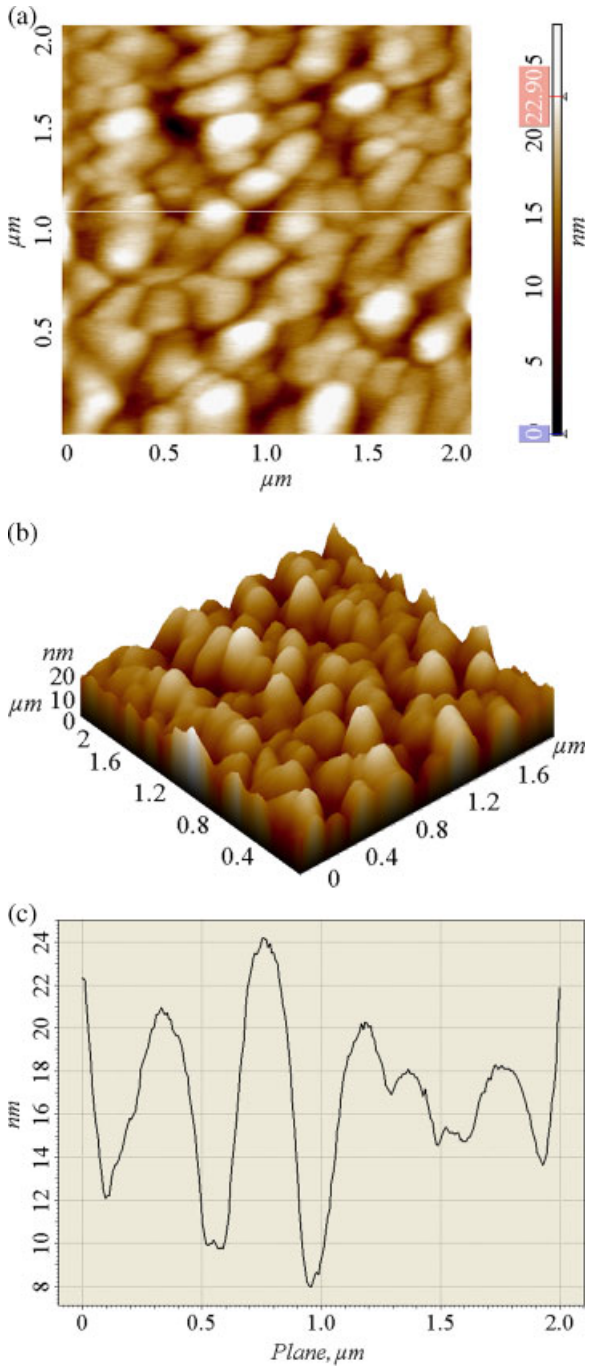

Fig 7. (a) The 2-D image of the same sample after annealing operations in which the sample was heated up to 400 °C. Thermal operation modifies the boundary of the grains. Electrical conductivity and optical properties improved, consequently. (b) and (c) 3-D image to show surface perspective and recorded fluctuations in a direction parallel to the *x*-axis shown in (a) to evaluate roughness.

images captured from just deposited and annealed films was compared using SPM.

References

Aggour M, Lewerenz HJ, Klaer J, Störkel U: Electrochemical processing of surface layers on $CuInS_2$ thin film solar cell absorbers. *Electrochem Solid-State Lett* **3**, 399–402 (2000).

Badeker K: Concerning the electricity conductibility and the thermoelectric energy of several heavy metal bonds. *Ann Phys* (*Leipzig*) **22**(4), 749 (1907).

Barabasi AL, Stanley HE: Fractal Concepts in Surface Growth, Cambridge University Press, New York (1995).

Bashar SA: Thesis, Study of indium tin oxide (ITO) for novel optoelectronic devices, University of London Regulations for the Degrees of M.Phil. and Ph.D., October (1997).

Bruce NC: Scattering of light from surfaces with one-dimensional structure calculated by the ray-tracing method. *J Opt Soc Am A* **14**, 1850–1858 (1997).

Chopra KL, Major S, Pandya DK: Transparent conductors—a status review. *Thin Solid Films* **102**, 1–46 (1983).

Fan JCC, Goodenough JB: X-ray photoemission spectroscopy studies of Sn-doped indium oxide films. *J Appl Phys* **48**(8), 3524–3531 (1977).

Guillen C, Herrero J: Polycrystalline growth and recrystallization processes in sputtered ITO thin films. *Thin Solid Films* **510**, 260 (2006).

Horák J, Loštak P, Drasa Č, Navra J, Uherc C: Defect structure of $Sb_{2-x}Fe_xTe_3$ single crystals. *J Solid State Chem* **180**, 915–921 (2007).

Hu Y, Diao X, Wang C, Hao W, Wang T: Effects of heat treatment on properties of ITO films prepared by rf magnetron sputtering. *Vacuum* **75**, 183 (2004).

Jafari GR, Fazeli SM, Ghasemi F, Vaez Allaei SM, Rahimi Tabar MR, *et al.*: Etched glass surfaces, atomic force microscopy and stochastic analysis. *Phys Rev Lett* **91**, 226101 (2003).

Jafari GR, Rahimi Tabar MR, Irajizad A, Kavei G: Etched glass surfaces, atomic force microscopy and stochastic analysis. *Physica A* **375**, 239–246 (2007).

Kerkach L, Layadi A, Dogheche E, Remiens D: Physical properties of RF sputtered ITO thin films and annealing effect. *J Phys D: Appl Phys* **39**, 184–189 (2006).

Minami T: Substitution of transparent conducting oxide thin films for indium tin oxide transparent electrode applications. *Inorg Chim Acta* **361**(3), 769–777 (2008).

Mohammadi Gheidari A, Behafarid F, Kavei G, Kazemzad M: Effect of sputtering pressure and annealing temperature on the properties of indium tin oxide thin films. *Mater Sci Eng B* **136**, 37–40 (2007).

Nath P, Bunshah RF: Preparation of In_2O_3 and tin-doped In_2O_3 films by a novel activated reactive evaporation technique. *Thin Solid Films* **69**, 63–68 (1980).

Terzini E, Thilakan P, Minarini C: Properties of ITO thin films deposited by RF magnetron sputtering at elevated substrate temperature. *Mater Sci Eng B* **77**, 110 (2000).

Tiwari AN, Pandya DK, Chopra KL: Analysis of the photovoltaic properties of sprayed $CuInS_2/SnO_X$:F solar cells. *Solar Energy Mater* **15**, 121–133 (1987).

Vassant Kumar CVR, Mansingh A: Effect of target–substrate distance on the growth and properties of rf-sputtered indium tin oxide films. *J Appl Phys* **65**, 1270 (1989).